



# Detailed Experimental and Model-Based Analysis of a Swash-Plate Piston Expander for ORC Application

Jean-François Oudkerk and Vincent Lemort\*

Thermodynamics Laboratory, Aerospace & Mechanical Engineering Department, University of Liège, Liège, Belgium

## OPEN ACCESS

### Edited by:

Andre Bardow,  
ETH Zürich, Switzerland

### Reviewed by:

Xiaofeng Guo,  
ESIEE Paris, France  
Paul Sapin,  
Imperial College London,  
United Kingdom

### \*Correspondence:

Vincent Lemort  
vincent.lemort@uliege.be

### Specialty section:

This article was submitted to  
Process and Energy Systems  
Engineering,  
a section of the journal  
Frontiers in Energy Research

**Received:** 19 July 2019

**Accepted:** 11 May 2020

**Published:** 26 June 2020

### Citation:

Oudkerk J-F and Lemort V (2020)  
Detailed Experimental and  
Model-Based Analysis of a  
Swash-Plate Piston Expander for ORC  
Application. *Front. Energy Res.* 8:107.  
doi: 10.3389/fenrg.2020.00107

A 195 cm<sup>3</sup> swash-plate piston expander was tested in an ORC using R245fa as working fluid. Rotational speeds ranging from 1,000 to 4,000 RPM and pressure ratios from 7 to 12 were imposed. In total, 65 steady state points were measured. With these measurements, performance maps were generated to point out the influence of rotational speed and levels of pressure on mechanical power and isentropic efficiency. These maps have highlighted the existence of an optimal rotational speed of around 3,000 RPM maximizing the mechanical power, while the speed that maximizes the isentropic efficiency lies between 2,000 and 2,500 RPM. The maximal mechanical power and isentropic efficiency were 2.8 kW and 53%, respectively. Then the measurements were used to analyze the losses. This analysis has shown that, under the expansion and compression limit, the theoretical isentropic efficiency has values comprised between 90 and 70% for pressure ratios of 7–12. The filling factor affects the isentropic efficiency for low rotational speeds and low pressure ratios. Indeed, indicated isentropic efficiency is around 60% for 1,000 RPM and around 75% for 4000 RPM. These values stay quite constant with the pressure ratio. Finally, a mechanical efficiency comprised between 40 and 90% was observed, which lowers the isentropic efficiency to values comprised between 30 and 53%. Finally, a model based on energy and mass conservation inside a cylinder volume was successfully calibrated and was able to predict mass flow rate, mechanical power, and exhaust temperature with good agreement. This model has enabled disaggregation of the influence of pressure drops and leakages on the filling factor, then on the isentropic efficiency. This analysis has shown that pressure drops mainly affect the compactness of the expander, and not so much the isentropic efficiency (except for low rotational speeds where pressure drops can lower the isentropic efficiency by 14%). In contrary, leakages have a strong impact. The importance of the different sources of losses varies with the speed. For the optimal speed of 2,500 RPM, under-expansion and compression have the strongest impact, followed by mechanical losses, leakages and pressure drops, respectively.

**Keywords:** ORC, piston expander, reciprocating expander, swash-plate expander, axial expander, R245fa

## INTRODUCTION

The piston expander, or reciprocating expander, is one of the major types of positive displacement expander. This type of machine converts the energy contained in a pressurized fluid into mechanical energy by increasing the volume of a working chamber, then decreasing the pressure of the fluid.

The piston expander is among the oldest displacement machines. It has been largely used during the Industrial Revolution and up to the beginning of the twentieth century. Piston expanders have been considered for several applications. In the 70's, piston expanders were used in cars powered by steam Rankine cycle systems. Then, at the beginning of the twenty-first century, in the context of the phase-out of several refrigerants, several studies proposed replacing the expansion valve of CO<sub>2</sub> compression cycles with small expanders in order to increase the COP of such systems. Recently, piston expanders have been increasingly considered for use in ORC applications, including micro-CHP applications and, more particularly, WHR on vehicle ICE engines. Piston expanders actually show some advantages over other expansion machines, such as a larger built-in volume ratio, high and achievable operating pressures and temperatures, their ability to ingest liquid and low rotational speeds.

Endo et al. (2007) tested a 7-cylinder, 185 cm<sup>3</sup> swash plate piston expander in an ORC integrated into a hybrid vehicle. Howell et al. (2011) investigated and tested a piston expander integrated into a RC for WHR on truck engines. Seher et al. (2012) tested a prototype of a single cylinder double acting piston with a total swept volume of 900 cm<sup>3</sup> for WHR on heavy duty vehicle engines (12,000 cm<sup>3</sup>). The authors also tested a micro-turbine and several fluids. They have concluded that the best technology is that of the piston with water or ethanol, or the turbine with ethanol. Daccord et al. (2013) designed and tested an oil-free single-cylinder piston expander of 443 cm<sup>3</sup>. The authors then developed a new prototype based on swash-plate technologies (Daccord et al., 2014). The expander has 5 cylinders for a total swept volume of 183 cm<sup>3</sup>. The last version of expander developed by these authors is larger, with a total swept volume of 300 cm<sup>3</sup> (Daccord and Sager, 2015). Galindo et al. (2015a,b) tested a 3-cylinder swash-plate piston expander integrated into an ORC using ethanol and coupled with a 2 l gasoline engine. Latz et al. (2013) used dimensional analysis and similarity parameters (specific speed and diameter) to select the expansion machine for an ICE WHR application. They concluded that piston expanders are best suited for heavy-duty vehicles. Later, Latz (2016) tested a 2-cylinder uniflow 760 cm<sup>3</sup> piston expander integrated into a RC system coupled with the EGR of a Volvo D13 heavy-duty diesel engine. Dingel et al. (2015) developed a prototype of piston expander for WHR on trucks. This prototype is a 350 cm<sup>3</sup> multi-flow engine with maximal inlet pressure and temperature of 50 bar and 270°C and a targeted power of 12 kW. Wronski et al. (2012) studied an innovative double-acting two-stage expansion reciprocating expander using pentane. Later, the authors tested a 730 cm<sup>3</sup> single-cylinder single-stage piston expander prototype in an ORC using n-pentane (Wronski, 2015). The admission system, consisting of a rotary valve, enabled the variation of the cut-off and two different camshafts allowed the testing of two

different exhaust timings. Galoppi et al. (2017) numerically and experimentally investigated a radial piston expander used in a R134a heat pump in place of a throttling valve. The machine was characterized by 9 cylinders and a total displacement of 102 cm<sup>3</sup>. The distribution system consisted of one stationary and one rotating plates. The timing of the different phases was determined by the overlapping of holes on both plates. The authors measured the impact of the inlet temperature, inlet quality and rotational speed on the fluid evolution inside the machine. Recently, Bianchi et al. (2019) experimentally investigated a prototype of piston expander made of 3 radial cylinders placed at 120°, equipped with rotary valves and with a total displacement of 230 cm<sup>3</sup>. The machine was integrated inside a micro-ORC working with R134a. It produced an electrical power ranging from 250 to 1200 W with an overall efficiency comprised between 38 and 42%.

Recently, piston expanders have often been compared with other volumetric expanders for use in small power ORC systems, whatever the application. Since 2013, several papers comparing expansion machines for ORC applications have shown that piston expanders are as good a candidate as scroll machines, screw machines and turbines (Bao and Zhao, 2013; Clemente et al., 2013; Lemort et al., 2013).

**Table 1** summarizes experimental works conducted on piston expanders. As can be seen, the size, type and operating conditions of piston expanders are comprised in a large range. Swept volumes vary from 26.5 cm<sup>3</sup> to 2,200 cm<sup>3</sup> for powers from 0.036 to 100 kW. Maximum values of inlet conditions range between 15 bar and 72 bar and temperatures from 30°C to 538°C.

This literature review indicates that there has been a large regain of interest for piston expanders during the last decade. Also, a large variety of mechanisms and working fluids have been investigated. The present paper aims first at supplementing the state of the art on piston expanders for ORCs, by describing an exhaustive experimental investigation conducted on a specific design of swash-plate piston expander, characterized by a total capacity of 195 cm<sup>3</sup> and fed with R245fa as working fluid. Second, the paper aims at proposing a detailed numerical/experimental analysis of piston expander performance by introducing relevant indicators, which clearly fills a gap in the current literature.

The paper is organized as follows. The second section of the paper defines the different performance indicators that will be used in the rest of the paper. The expander and the test bench are then described, as well as the ORC control strategy. Measurements are then used to establish performance maps of the expander and to analyze the different sources of losses. Finally, a comprehensive model is proposed, calibrated and used to disaggregate the influence of leakages and pressure drops on the efficiency.

## PERFORMANCE INDICATORS

In order to assess and compare the performance of volumetric expanders, performance indicators must be defined. In this section, the well-known filling factor and isentropic efficiency are defined and disaggregated into several indicators in order to

**TABLE 1** | Piston expander experimental studies summary.

References	Application	Size (cm <sup>3</sup> )	Type	Admission system actuation	Maximal operating conditions	Power/Isentropic efficiency
Technologie Assesment Evaluation Branch (1974)	Steam car	2,200	Uniflow	Cam	69 bar 538°C	100 kW -
Baek et al. (2002)	CO2 compression cycle	26.5	Adapted 2 cylinders ICE	Solenoid	72.5 bar 30°C	0.036 kW 11%
Zhang et al. (2007)	CO2 compression cycle	36.8	Free-piston, Double acting piston	Sliding valves	54.5 bar -	-
Endo et al. (2007)	Vehicle WHR, RC	185	7 cylinders Swash plate	Rotary valves	60 bar 450°C	3 kWel -
Seher et al. (2012)	Vehicle WHR, RC	900	Double acting piston	Sliding valve	32 bar 380°C	14 kW -
Daccord et al. (2013)	Vehicle WHR, RC	443	1 cylinder Uniflow/Cross-flow/ Multiflow	Cam	36 bar -	2 kWel 54%
Daccord et al. (2014)	Vehicle WHR, RC	183	5 cylinders Swash plate Uniflow	Camless	29 bar 300°C	3.6 kW
Daccord and Sager (2015)	Vehicle WHR, ORC ethanol	300	6 cylinders Swash plate Uniflow	Cam	37 bar 230°C	9.5 kW 56%
Galindo et al. (2015a,b)	Vehicle WHR, ORC ethanol	117	3 cylinders Swash plate Uniflow		28.7 bar 200°C	1.83 kW 58 %
Latz et al. (2015)	Vehicle WHR, RC	760	2 cylinders Uniflow	Cam	30 bar 300°C	2.6 kW -
Wronski (2015)	Micro-CHP n-pentane	730	1 cylinder	Rotary valve	15 bar 150°C	2.5 kW 74 %
Galoppi et al. (2017)	R134a heat pump	102	9 cylinders	Rotary valve	16,9 bar 60°C	-
Bianchi et al. (2019)	WHR ORC, R134a	230	3 cylinders	Rotary valves	17 bar 85°C	1,200 W 42%

distinguish the effect of each source of losses. A third indicator is also proposed to quantify the compactness of an expander.

## Volumetric Performance

As for volumetric compressors, the volumetric performance of a positive displacement expander is evaluated with the ratio between the actual and theoretical mass flow rates (called filling factor):

$$\phi = \frac{\dot{M}}{\dot{M}_{th}} \quad (1)$$

However, contrary to compressors, the leakage flows have the same direction as the internal flow and tend to increase the total mass flow rate absorbed by the machine, and consequently the filling factor. Hence, the effects of the leakages and the pressure drops are antagonistic. Moreover, the fluid cooling down during the suction process can also lead to an increase in the entering fluid mass flow rate. These different antagonistic effects make analysis of the filling factor difficult. To better quantify and understand the separate effect of leakages, the filling factor can be disaggregated into two parts:

$$\phi = \frac{\dot{M}}{\dot{M}_{th}} = \frac{\dot{M}}{\dot{M}_{in}} \cdot \frac{\dot{M}_{in}}{\dot{M}_{th}} = \phi_l \cdot \phi_{in} \quad (2)$$

In this equation,  $\phi_l$  is the leakage filling factor and quantifies the effect of the leakages.  $\phi_{in}$  is the internal filling factor and quantifies the effect of supply pressure drop and heat transfer. The leakage filling factor is greater than unity, while the internal filling factor is smaller than unity if pressure drops are predominant.

## Energy Conversion Efficiency

In order to assess the performance of the expansion machine, the produced power is compared to the power produced for a reference fluid evolution under the same operating conditions (supply condition and exhaust pressure) and with the same mass flow rate. The reference evolution is an isentropic evolution (adiabatic and reversible) and the ratio between the actual power and the isentropic power is defined as the isentropic efficiency. Considering the indicated power, the indicated isentropic efficiency is given by:

$$\epsilon_{s,in} = \frac{\dot{W}_{in}}{\dot{W}_s} = \frac{\dot{W}_{in}}{\dot{M} \cdot (h_{su} - h_{ex,s})} = \frac{\dot{W}_{in}}{\dot{M} \cdot \Delta h_s} \quad (3)$$

where  $h_{ex,s}$  is the fluid-specific enthalpy at the exhaust of the expander if the expansion was isentropic. Alternatively,

considering the shaft power, the shaft isentropic efficiency can be defined as:

$$\epsilon_{s,sh} = \frac{\dot{W}_{sh}}{\dot{W}_s} = \frac{\dot{W}_{sh}}{\dot{W}_{in}} \cdot \frac{\dot{W}_{in}}{\dot{M} \cdot \Delta h_s} = \eta_m \cdot \epsilon_{s,in} \tag{4}$$

Both indicated and shaft isentropic efficiencies are related by the mechanical efficiency  $\eta_m$ .

As for the filling factor, the shaft isentropic efficiency can be disaggregated in order to assess the relative impact of each source of losses:

$$\begin{aligned} \epsilon_{s,sh} &= \frac{\dot{W}_{sh}}{\dot{m} \cdot \Delta h_s} = \frac{\dot{W}_{sh}}{\dot{W}_{in}} \cdot \frac{\dot{W}_{in}}{\dot{W}_{in,th}} \cdot \frac{\dot{W}_{in,th}}{\dot{M}_{th} \cdot \Delta h_s} \cdot \frac{\dot{M}_{th}}{\dot{M}_{in}} \cdot \frac{\dot{M}_{in}}{\dot{M}} \\ &= \eta_m \cdot \epsilon_{in} \cdot \epsilon_{s,th} \cdot \frac{1}{\phi_{in}} \cdot \frac{1}{\phi_l} \end{aligned} \tag{5}$$

All the factors of this decomposition have already been defined, except:

- The theoretical isentropic efficiency  $\epsilon_{s,th}$ , which quantifies the under- or over- expansion and compression losses (see **Figure 1**).
- The diagram factor  $\epsilon_{in}$ , which quantifies the effect of the irreversibilities (pressure drops and heat transfer) on the indicated power (see **Figure 1**).

As explained above, the mechanical efficiency  $\eta_m$  quantifies the mechanical losses and the last two factors account for the impact of losses on the mass flow rate.

In Equation (5), two factors account for pressure drops and heat transfer effects: the diagram factor  $\epsilon_{in}$  and internal filling factor  $\phi_{in}$ . Consequently, the collective effect of pressure drops and heat transfer on isentropic efficiency is given by:

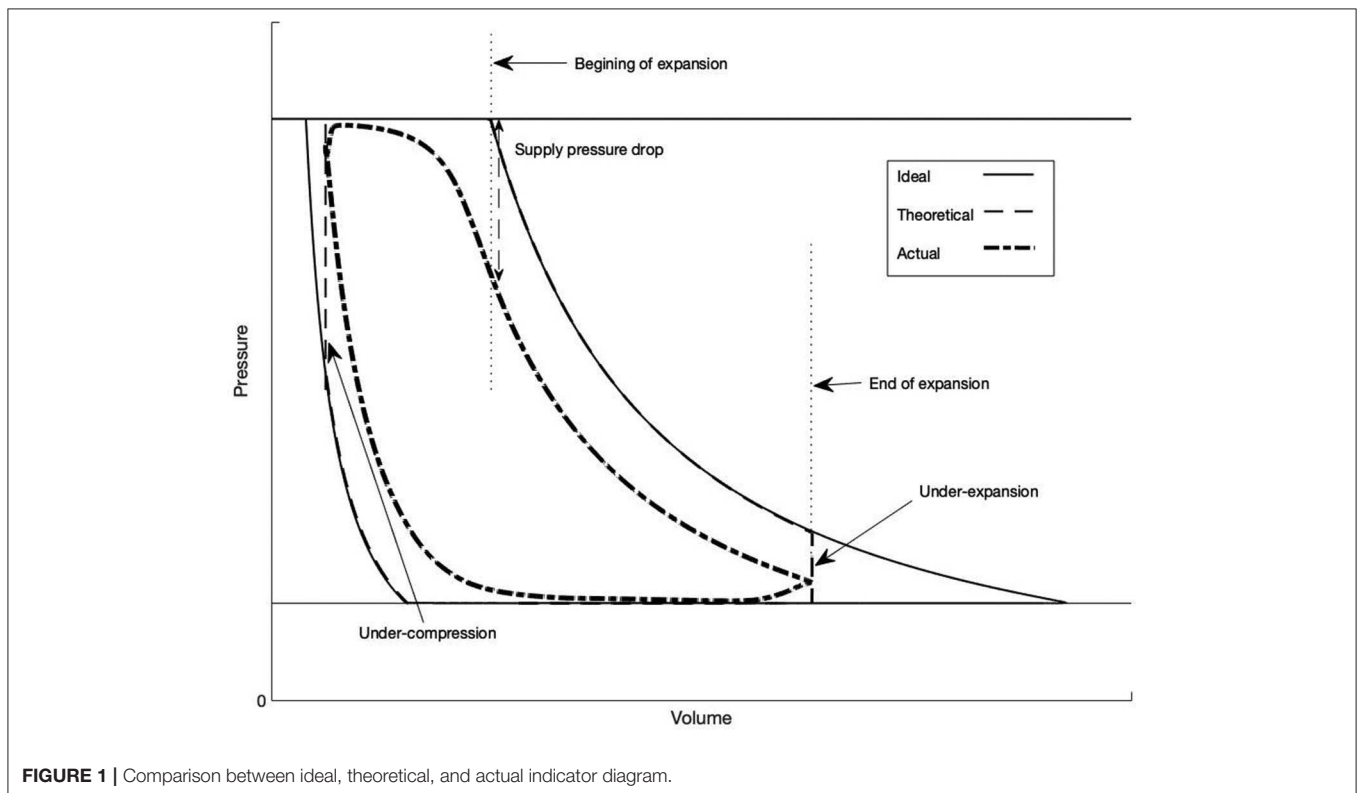
$$\epsilon_{sp,in} = \frac{\epsilon_{in}}{\phi_{in}} = \frac{\dot{W}_{in}}{\dot{M}_{in}} \cdot \frac{\dot{M}_{th}}{\dot{W}_{in,th}} = \frac{w_{in}}{w_{in,th}} \tag{6}$$

and corresponds to the ratio between indicated and theoretical specific works and it will be called “specific diagram factor”. It is interesting to note that, as internal filling factor is more often smaller than unity, it tends to increase the isentropic efficiency. However, this increase does not stem from an improvement, but from the reduction of the mass flow rate used to compute the isentropic efficiency.

This disaggregation allows for the evaluation of the impact of the different sources of losses and the comparison of different volumetric expanders. The values of the factors of these losses can be obtained by experimentation and/or modeling. Theoretical isentropic efficiency is always determined by modeling. Mechanical efficiency and diagram factor can be measured if in-cylinder pressure measurements are available to compute indicated work. Finally, as leakages are difficult to measure, it is more convenient to simulate them to obtain leakage and internal filling factors.

### Compactness

In order to quantify the compactness of a piston expander, the delivered power can be divided by the displaced volume. As



shown in Equation (7), the compactness is the product of the rotational speed  $N$ , the mechanical efficiency  $\eta_m$ , the diagram factor  $\epsilon_{in}$  and the ratio between the theoretical indicated work and the displaced volume. The latter factor has the dimensional unit of a pressure and is called “theoretical indicated mean effective pressure”.

$$C_{ness} = \frac{\dot{W}_{sh}}{V_{tot}} = N \cdot \frac{W_{sh}}{W_{in}} \cdot \frac{W_{in}}{W_{in,th}} \cdot \frac{W_{in,th}}{V_{tot}} = N \cdot \eta_m \cdot \epsilon_{in} \cdot imep_{th} = N \cdot \eta_m \cdot imep = N \cdot smep \tag{7}$$

As for the theoretical indicated mean effective pressure, the “indicated mean effective pressure” and “shaft mean effective pressure” can be defined as:

$$smep = \frac{W_{sh}}{V_{tot}} = \eta_m \cdot imep = \eta_m \cdot \epsilon_{in} \cdot imep_{th} \tag{8}$$

In the same way, mechanical losses are sometimes expressed as “friction mean effective pressure”:

$$fmep = \frac{W_{loss}}{V_{tot}} \tag{9}$$

## DESCRIPTION OF THE TEST BENCH

### Piston Expander

The tested expander is a prototype of a swash-plate piston machine with five cylinders and characterized by a total swept volume of 195 cm<sup>3</sup> (piston bore and stroke: 40 and 31 mm, respectively) and by a clearance volume of 32.81 cm<sup>3</sup>. The exhaust ports are located in the lower part of the cylinders and are piston-controlled (the pistons cover and uncover the ports). The supply port is located in the head of the cylinders and is actuated with a camless system (see **Figure 2**). These two systems induce symmetrical opening and closing compared to TDC and BDC. As the inlet port is on the head of the cylinder and the exhaust port are on the other side of the cylinder, the expander shows a “uniflow” configuration. Other geometrical parameters of the expander are given in **Supplementary Table 2**.

The lubrication of the expander is ensured by an external oil loop with injection of oil at main friction points (see **Figure 2**). The oil loop is composed of a tank, pump and oil cooler. The latter system allows for the lubricant to be cooled.

Finally, in order to dissipate the produced power, the shaft of the expander is connected, via a torque meter and two elastic couplings, to an asynchronous generator. This generator is controlled by a four-quadrant variable frequency drive.

### ORC Set Up

The piston expander is integrated into an ORC cycle test bench using R245fa as the working fluid. The test bench has been described by Dickes et al. (2014). It is composed of a pump, a re-cuperator, a boiler, a condenser and a liquid tank. The boiler is fed with thermal oil heated by electrical resistances and the condenser is water-cooled. A by-pass line allows the evaporator to be heated and pressurized by bypassing the expander. It is also used to start feeding the expander by closing the line and opening the inlet of the expander.

### Measurement System

Several sensors are placed all over the ORC system and the expander set-up in order to measure the performance of the expander. The working fluid flow rate is measured at the pump outlet by a Coriolis-effect mass flow meter. The temperature and the pressure of the working fluid at the inlet and the outlet of each component of the ORC are measured with thermocouples and piezoresistive pressure sensors, respectively. The same types of sensors, as well as flow meters, are also placed on the oil loop and water loop in order to compute the heat power rejected by the lubricant. The torque, measured by a torque-meter placed between the expander and the generator, and the rotational speed given by the drive allow the mechanical power to be computed. In addition to these measurements, the pressure in one of the cylinders is measured by means of a piezoelectric pressure sensor and the angular position of the shaft with a rotary encoder. This measurement system allows the indicator diagrams to be drawn, and thus the indicated power and the mechanical efficiency to be computed.

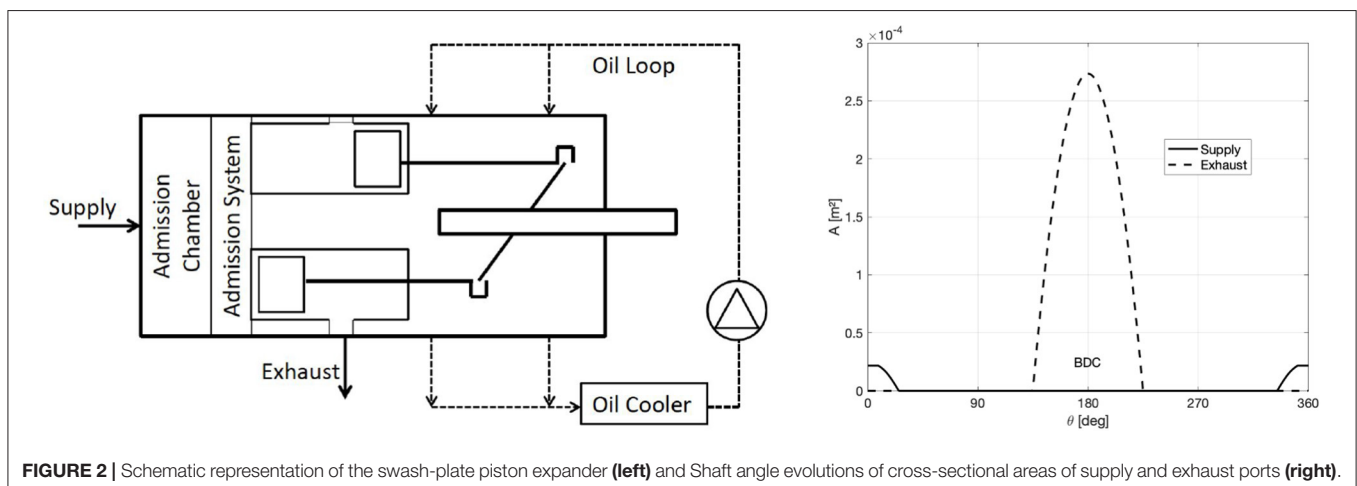


**FIGURE 2** | Schematic representation of the swash-plate piston expander (left) and Shaft angle evolutions of cross-sectional areas of supply and exhaust ports (right).

Table 2 lists the locations, types, ranges and uncertainties of sensors.

### Control of the Operating Parameters

On the working fluid side, the system has four degrees of freedom:

- The rotational speed of the expander, controlled by the variable frequency drive of the asynchronous generator.
- The mass flow rate of the working fluid and thus the supply pressure, controlled by the rotational speed of the pump.
- The expander supply temperature and thus the superheating, controlled by the electric oil boiler.
- The expander exhaust pressure, controlled by a throttling valve on the exhaust line.

The superheating was kept between 6 and 15 K, the supply pressure between -1.2 and +1.6% of the set value and the exhaust pressure between -2.1 and +2.9%.

TABLE 2 | Sensors characteristics and location.

Type	Range	Error
Class 2 K type thermocouple	-40 to 1,200°C	[-40 to 333]: ±2.5°C; [333 to 1,200°C]: ±0.75%*
Class 2 T type thermocouple	-40 to 350°C	[-40 to 133]: ±1°C; [133 to 350°C]: ±0.75%*
Piezoresistive pressure sensor	0 to 16 bar	0.5%
Piezoelectric pressure sensor	0 to 344 bar	1%
Strain gage torque meter	-20 to 20 Nm	1% FS
Coriolis flow working fluid flow meter	0 to 155 g/s	0.1%
Epicycloid wheel oil flow meter	0.06 to 16 l/m	1.25%
Wheel counter water flow meter	/	2%

\* EN60584 (Subcommittee, 65B: Measurement and Control Devices, 2013).

## EXPERIMENTAL RESULTS

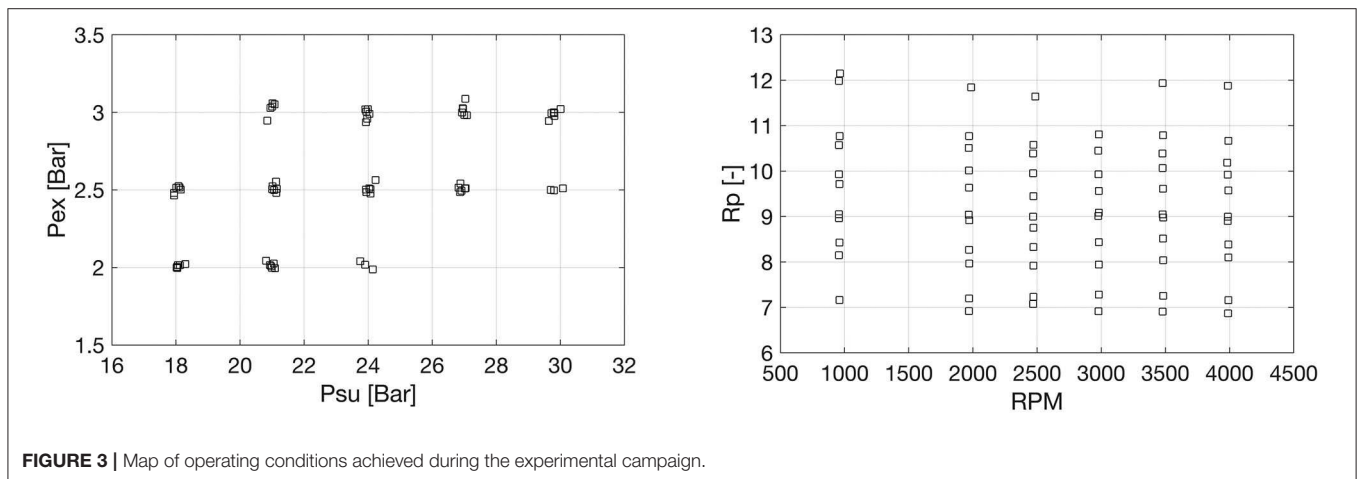
The piston expander was tested under a wide range of operating conditions. Indeed, supply pressure varied from 18 to 30 bar, exhaust pressure varied from 2 to 3 bar and rotational speed from 1,000 to 4,000 RPM. A total of 65 steady-state points have been measured in these ranges. The validity and the quality of the experimental results are presented in the **Supplementary Table 1**. Raw measurement data, calculated values, uncertainties and reconciliated values are given in **Supplementary Table 2**.

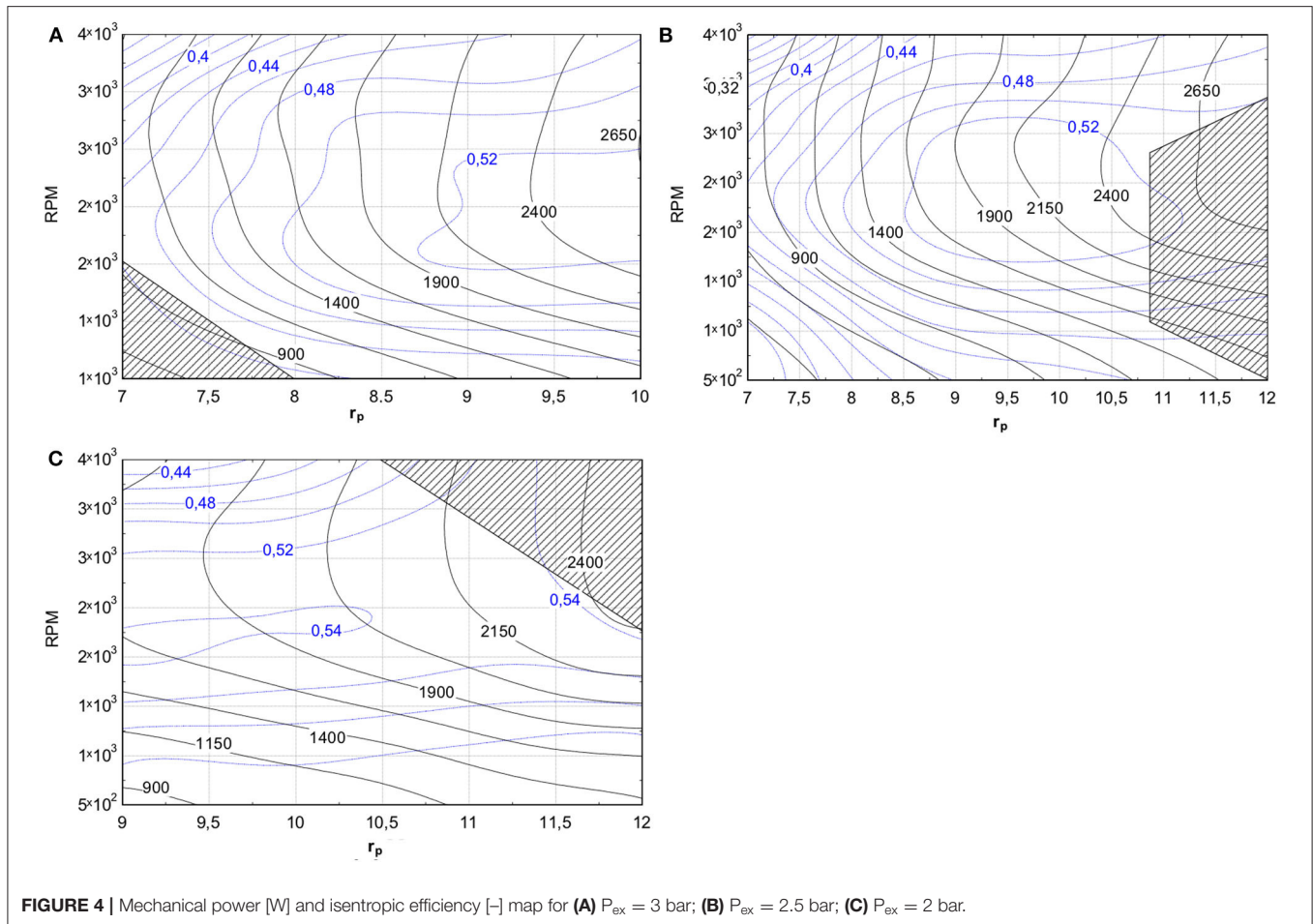
Figure 3 shows exhaust pressure in terms of supply pressure and pressure ratio ( $R_p$ ) in terms of rotational speed to illustrate the operating conditions.

Figure 4 shows maps of mechanical power and isentropic efficiency [computed with Equation (4)]. On these maps, the hatched area represents the operating conditions that have not been investigated.

It can be observed that mechanical power increases with the pressure ratio and that there is an optimal value of rotational speed around 3,000 RPM that maximizes the mechanical power. This optimum is due to antagonistic effects: the impact of leakages decreases with the rotational speed while mechanical losses increase with the rotational speed. The comparison of the three maps shows that, for the same pressure ratio, the mechanical power is higher for higher levels of pressure. Over the 65 points, the power varies between 392 W (for  $P_{su} = 18$  bar,  $P_{ex} = 2.5$  bar and  $RPM = 1000$ ) 2847 W (for  $P_{su} = 30$  bar,  $P_{ex} = 2.5$  bar and  $RPM = 2000$ ).

The isentropic efficiency increases up to a pressure ratio of around 9 and then seems to stabilize at a value between 52 and 54%, depending on the exhaust pressure. As for mechanical power, there is an optimal rotational speed that maximizes the isentropic efficiency. This optimal rotational speed is between 2,000 and 2,500 RPM. Over the 65 points, the isentropic efficiency varies from 30.85% (for  $P_{su} = 18$  bar,  $P_{ex} = 2.5$  bar and  $RPM = 4000$ ) to 54.12% (for  $P_{su} = 18$  bar,  $P_{ex} = 2$  bar and  $RPM = 2000$ ).





## Indicator Diagram

As mentioned above, in-cylinder pressure sensors allowed the in-cylinder pressure to be measured, then indicator diagrams to be drawn and indicated work and power computed. The indicated work and power were used in the previous section to split the losses and compute mechanical efficiency. Over the 65 points, the indicated work of one cylinder varies from 5.3 W (for  $P_{su} = 18$  bar,  $P_{ex} = 2.5$  bar and  $RPM = 4000$ ) to 27.9 W (for  $P_{su} = 30$  bar,  $P_{ex} = 2.5$  bar and  $RPM = 1000$ ).

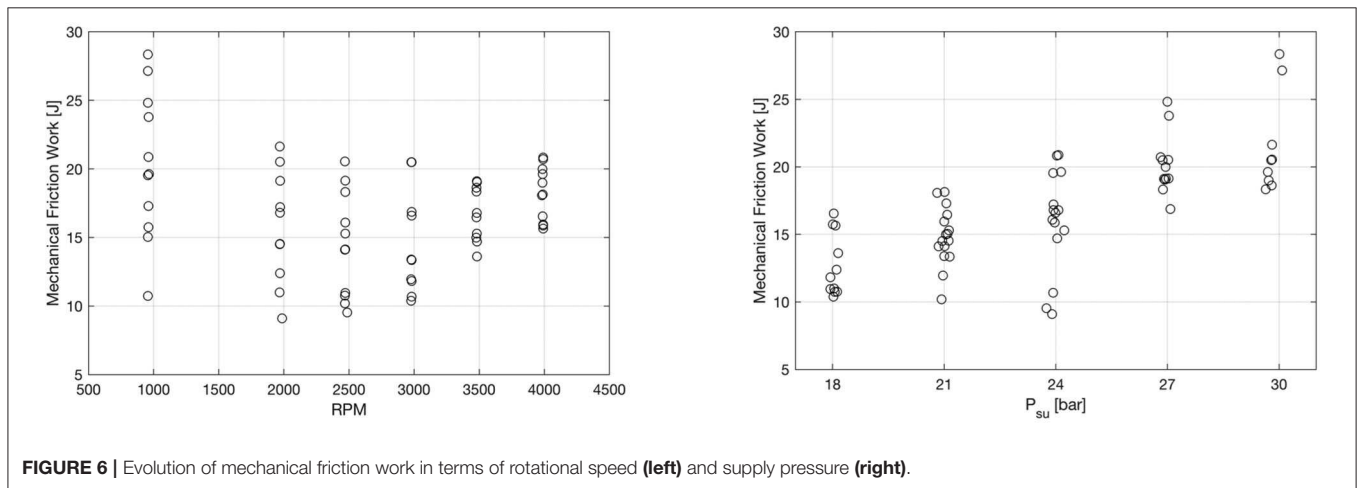
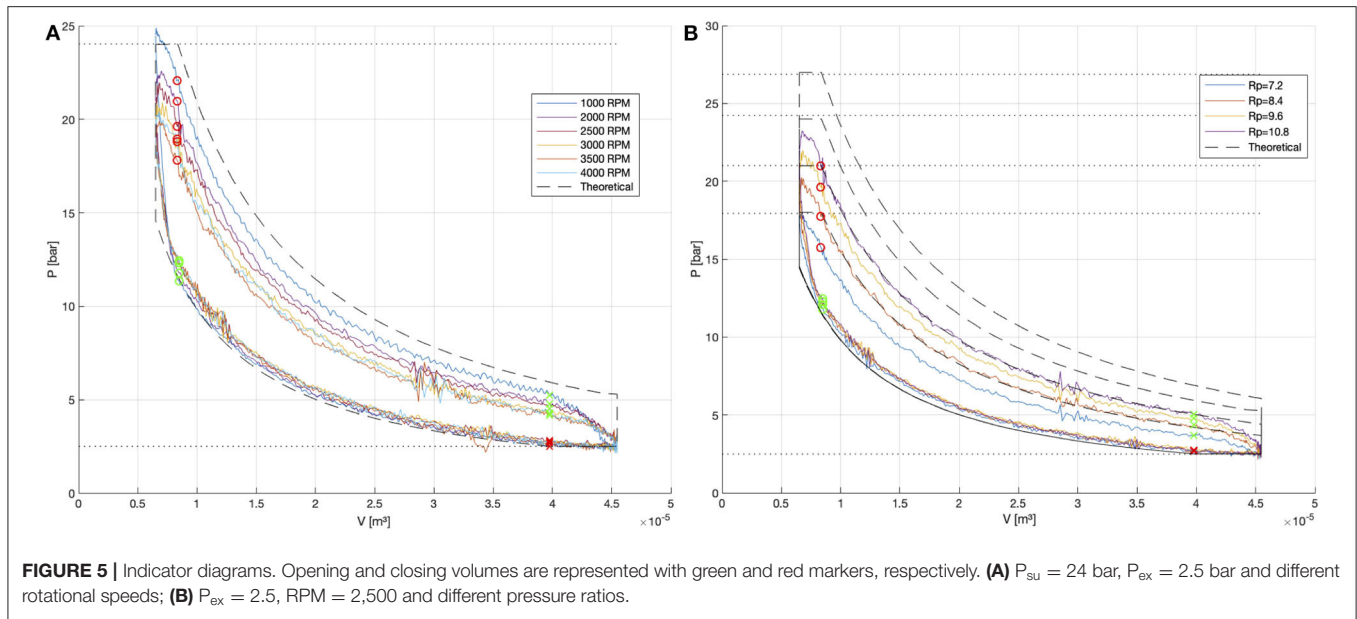
**Figure 5** shows indicator diagrams for different operating conditions. **Figure 5A** shows the effect of the rotational speed on the indicator diagram for a supply pressure of 24 bar and an exhaust pressure of 2.5 bar. It can be seen that the indicator diagram is fairly close to the theoretical one for 1,000 RPM (the factor diagram  $\epsilon_{in}$  is comprised between 70 and 80% depending on the pressure ratio). Supply pressure drops are the most considerable losses and increase significantly with the speed. In-cylinder pressure at inlet closing volume (red circles) passes from 22 bar to 17 bar for rotational speed increasing from 1,000 to 4,000 RPM and  $\epsilon_{in}$  decreases from 78 to 43%. Exhaust pressure drops are less significant but induce a compression process at a slightly higher pressure than the theoretical one. Finally, early opening of supply/exhaust ports induces an early rise/fall in pressure before the piston reach TDC/BDC.

**Figure 5B** shows the effect of pressure ratio. It can be seen that supply pressure drops also increase with pressure ratio, because points characterized by higher pressure ratios are achieved with higher mass flow rates. The ratio between in-cylinder pressure at inlet closing volume (red circles) and supply pressure passes from 0.87 to 0.77 for pressure ratio increasing from 7.2 to 10.8. This increase in supply pressure drops causes the diagram factor  $\epsilon_{in}$  to decrease from 57 to 54%.

## Mechanical Losses

As the indicated and shaft powers are both known, the mechanical friction work and power can be computed. **Figures 6, 7** show the evolution of these two values in terms of rotational speed and supply pressure. It can be seen that the mechanical friction work can increase when the rotational speed decreases. This leads to the conclusion that boundary lubrication regime is encountered, especially at low rotational speed. Moreover, it seems that the mechanical friction work is better correlated with the supply pressure (and then the load) but still scattered. This boundary regime can be explained by inappropriate oil characteristics, which are influenced by the temperature and the amount of diluted working fluid.

It can be observed that mechanical friction power is (unlike the work) well correlated with the rotational speed. However, supply pressure seems to have a significant impact. Thus



a correlation including the rotational speed and the supply pressure is proposed:

$$\dot{W}_{mf} = 0.0646 N^2 + 0.552 N.P_{su} \quad (10)$$

where  $\dot{W}_{mf}$  is the mechanical friction power in [W],  $N$  is the rotational speed in [Hz] and  $P_{su}$  is the supply pressure in [bar]. The first term accounts for the hydrodynamic friction while the second one stands for the boundary friction. This correlation predicts the mechanical friction power with a coefficient of determination of 89%. The corresponding  $f_{mep}$  is:

$$f_{mep} = 5.5 \cdot 10^{-5} RPM + 0.0283 P_{su} \quad (11)$$

with  $f_{mep}$  and  $P_{su}$  in [bar].

### Measurements-Based Losses Analysis

As shown in section Performance indicators, different kinds of losses affect the isentropic efficiency and it is possible to split the latter in order to disaggregate the effect of each of the losses. **Figure 8** illustrates the disaggregation of the isentropic efficiency of the tested expander.

As explained previously, the theoretical isentropic efficiency only accounts for the under-expansion and compression losses. Starting with a full isentropic process, under-expansion and compression affect the isentropic efficiency of the theoretical indicator diagram. It can be seen in **Figure 8A** that these losses limit the isentropic efficiency at values between 70 and 90% and, as expected, increase with pressure ratio.

Pressure drops and heat transfer then tend to decrease the indicated power compared to the theoretical power. The ratio between the actual and the theoretical indicated power (diagram factor) is shown in **Figure 8B**. This ratio varies from 0.35 to 0.8

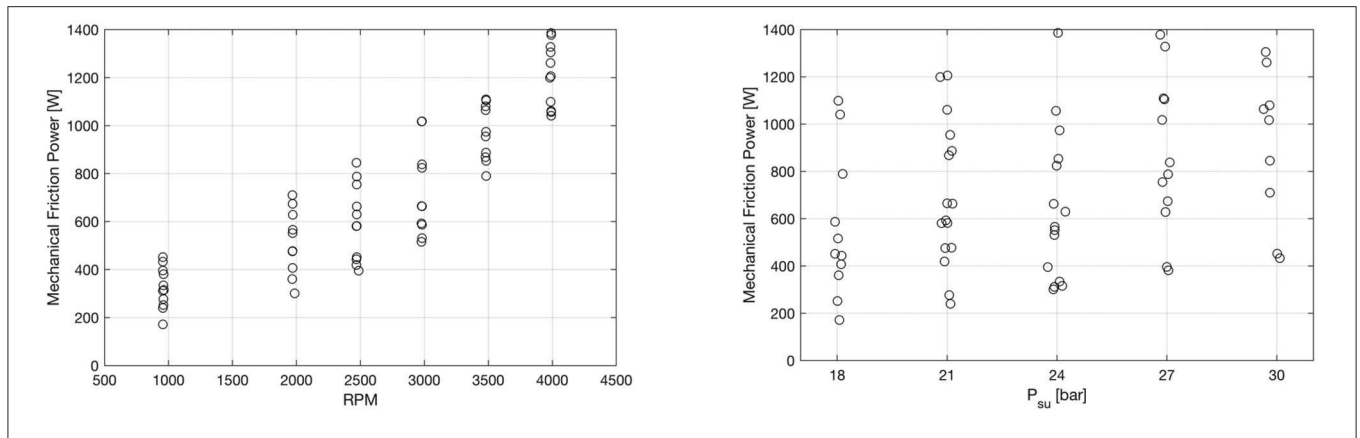


FIGURE 7 | Evolution of mechanical friction power in terms of rotational speed (left) and supply pressure (right).

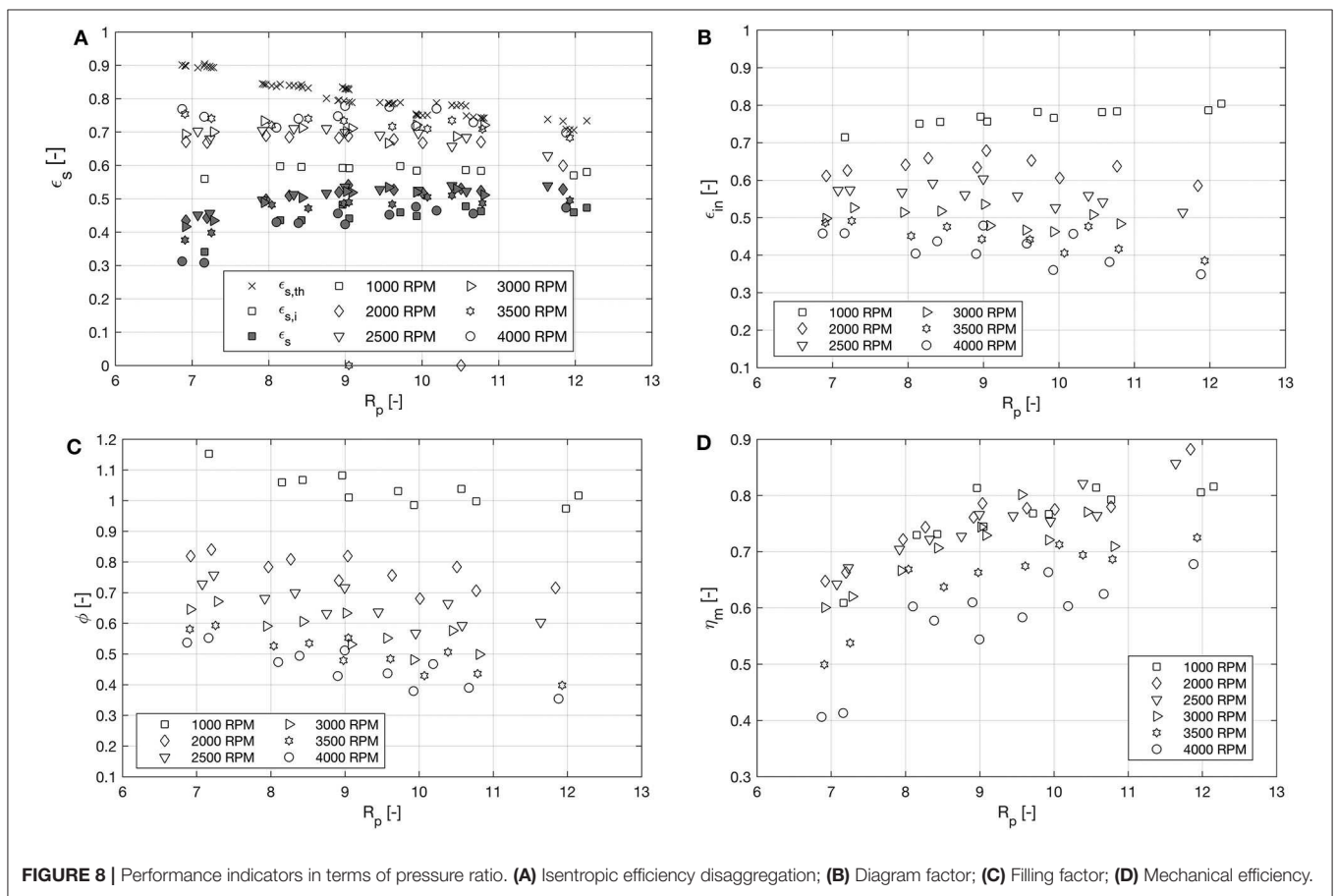


FIGURE 8 | Performance indicators in terms of pressure ratio. (A) Isentropic efficiency disaggregation; (B) Diagram factor; (C) Filling factor; (D) Mechanical efficiency.

and decreases with the rotational speed because of the increase in the pressure drops with the speed. The effect of the speed and pressure ratio on the pressure drop and then on the indicator diagram has been illustrated in the previous section (Figure 5).

Figure 8C shows the evolution of the filling factor with the pressure ratio and speed. It can be seen that the filling factor decreases with the speed. This decrease is due to the increase of the pressure drop and the decrease of the impact of the leakages.

Indeed, the leakage flow rates are rather independent of the rotational speed. Consequently, they have more impact at low rotational speed, as the mass flow rate displaced by the expander is itself lower. As already mentioned in section Performance indicators, a reduction of the filling factor leads to an increase in the isentropic efficiency by decreasing the reference mass flow rate. This is why indicated isentropic efficiency rises with the speed despite the decrease in the diagram factor. Filling

factor also decreases with pressure ratio, increasing the indicated isentropic efficiency for low pressure ratios. Indeed, **Figure 8A** shows that the difference between theoretical and indicated isentropic efficiencies is larger at low pressure ratios. As explained in section Performance indicators, filling factor depends on two antagonistic effects: pressure drops and leakages, which tend to decrease and increase the filling factor, respectively. These effects cannot be analyzed with the measurement but will be analyzed with the model.

Finally, mechanical losses affect the shaft power. It can be seen that mechanical efficiency decreases with the rotational speed (see **Figure 8D**), counterbalancing the effect of the leakages. These two opposite effects on the isentropic efficiency yield an optimal rotational speed of around 2,000–2,500 RPM, as observed in the previous section (see **Figure 4**). It can be seen in **Figure 8A** that isentropic efficiency decreases for low pressure ratios. Indeed, when pressure ratio decreases, indicated power also decreases but constant mechanical losses remain present, leading to a decrease in the mechanical efficiency (see **Figure 8D**). As shown in **Figure 8D**, mechanical efficiency varies from 40 to 90%.

## COMPREHENSIVE MODEL DESCRIPTION

The proposed comprehensive model of piston engine is based on the conservation of energy and mass in the control volume, defined by the cylinder wall and the piston. The goal of the model is to compute the crank angle evolution of the fluid state. In the proposed model, three assumptions are introduced:

- The pressure of the fluid is homogeneous inside the cylinder.
- The temperature is the mass-average temperature inside the cylinder.
- The temperature of the cylinder walls is uniform.

In order to compute the state of the fluid, a geometrical model is needed to define the volume of the open system defined by the control volume boundaries and the cross-sectional areas of the inlet and exhaust ports. A heat transfer model is proposed to compute the heat transfer rate between the fluid and the wall. Then, the supply and exhaust flows must be computed as a function of the upstream and downstream pressures. Conservation of energy and mass, coupled with fluid state model, allows the state of the fluid inside the cylinder to be computed. Finally, values such as average mass flow rate, indicated power and exhaust temperature averaged over one revolution can be computed.

The goal of the geometric model is to express the cylinder volume in terms of the shaft angle  $\theta$ . This volume can be expressed as:

$$V = V_0 + \pi \cdot \frac{D^2}{4} \cdot x \quad (12)$$

where  $V_0$  is the clearance volume,  $D$  is the bore diameter and  $x$  is the distance between the TDC and the piston head. The expression of this last value depends on the linear to rotation motion conversion system. For the crankshaft system, Equation

(13) can be used and for swash or wobble plate, this distance is given by Equation (14).

$$x = B + \frac{L}{2} \cdot (1 - \cos(\theta)) - \sqrt{B^2 - \left(\frac{L}{2}\right)^2 \cdot \sin^2(\theta)} \quad (13)$$

$$x = \frac{L}{2} \cdot (1 - \cos(\theta)) \quad (14)$$

where  $B$  is the length of the connecting rod,  $R$  is the crank radius and  $L$  the piston stroke.

The calculation of a port cross-sectional area depends on the valve type (poppet valve, sliding valve, etc.) and dimensions. For each machine, valve dimensions and motion must be defined. However, poppet valves with cam actuation are a widespread system and a generic equation for valve lift and cross section can be found in the literature.

For poppet valves, the cross-sectional area depends on the dimensions of the valve head, seat and stem and can be computed according to (Heywood, 1988).

The valve lift depends on the cam profile and on the dynamic behavior of the valve train. Indeed, some deformations, rebound, etc. can appear when the valve train is in motion, making the dynamic lift different from the kinematic lift. Blair (1999) proposed a general description of cam-actuated valve lift based on five parts: ramp up, main lift up, dwell, main lift down and ramp down.

## Heat Transfers

The fluid inside the cylinder is at a temperature different to those of the cylinder wall and piston head, and then exchanges heat with them. Considering a uniform temperature of the fluid and the wall, the heat flux exchanged by the fluid can be expressed as:

$$\dot{Q}_w = h_c \cdot S_w \cdot (T - T_w) \quad (15)$$

where  $h_c$  is the convective heat transfer coefficient,  $S_w$  the area of the cylinder wall and piston head and  $T_w$  the uniform temperature of this wall.

The convective heat transfer coefficient  $h_c$  can be estimated through several correlations that give the Nusselt number. Different correlations can be found in literature for piston machines such as ICE or reciprocating compressors. These correlations allowing computation of the Nusselt number are most often in the form of Equation (16).

$$Nu = a \cdot Re^b \cdot Pr^c \quad (16)$$

where  $Re$  and  $Pr$  are the Reynolds and the Prandtl numbers, respectively. The correlations differ by the values of the constants  $a$ ,  $b$  and  $c$  and by the choice of the characteristic length  $L_c$  and the fluid speed  $C$  used to compute the Reynolds number. These values are presented in **Table 3** for three correlations. Woschni's correlation has been selected.

## Mass Flow Rates

In order to solve the mass and energy conservation equations, the mass flows entering and leaving the control volume must be known. In the proposed model, the different orifices are treated

**TABLE 3 |** Heat transfers correlation parameters values.

Authors	Parameters values	Original application
Woschni (1967)	$a = 0.035$ $b = 0.8$ $c = 0$	ICE
	$L_c = D$ $C_p = 6.18(2.L \cdot \frac{\omega}{2\pi})$ gas exchange $C_p = 2.28(2.L \cdot \frac{\omega}{2\pi})$ expansion and compression	
Annand (1963)	$a = 0.35$ $b = 0.7$ $c = 0$	ICE
	$L_c = D$ $C_p = 2.L \cdot \frac{\omega}{2\pi}$	
Adair et al. (1972)	$a = 0.053$ $b = 0.8$ $c = 0.6$	Reciprocating compressor
	$L_c = D$ $C_p = 2.L \cdot \frac{\omega}{2\pi}$	

as convergent nozzles and flows are assumed to be isentropic. The mass flow rates are then computed by the following equation:

$$\dot{m} = C_d \cdot A_v \cdot \rho_{thr} \sqrt{2 \cdot (h_{up} - h_{thr})} \tag{17}$$

where  $A_v$  is the cross flow area,  $h_{up}$  is the enthalpy of the upstream fluid and  $h_{thr}$  and  $\rho_{thr}$  are the enthalpy and the density at the throat of the nozzle. The state of the fluid at the throat of the nozzle is computed assuming isentropic flow from the supply to the throat and therefore with the entropy of the upstream fluid. Considering that the flow can be choked, the pressure at the nozzle throat is:

$$\text{If } P_{down} > P_{crit} : P_{thr} = P_{down} \tag{18}$$

$$\text{If } P_{down} < P_{crit} : P_{thr} = P_{crit}$$

where  $P_{down}$  is the downstream pressure and  $P_{crit}$  is the critical value of the downstream pressure at which the flow becomes choked. Assuming a perfect gas, this critical value is:

$$P_{crit} = P_{up} \cdot \left( \frac{2}{\gamma + 1} \right)^{\frac{\gamma}{\gamma - 1}} \tag{19}$$

where  $\gamma = c_p/c_v$  is the isentropic coefficient.

Leakage mass flow rates are computed in the same way, with a fictitious lumped cross-sectional area by-passing the cylinder.

### Conservation Equations and Derivation of Differential Equations Governing the Process

The boundaries of the volume defined above form an open thermodynamic system. The conservation of energy principle applied to a control volume is:

$$\frac{dE}{dt} = \dot{Q} + \dot{W} + \sum \dot{m}_{su} \cdot \left( h + \frac{C^2}{2} + g \cdot z \right)_{su} - \sum \dot{m}_{ex} \cdot \left( h + \frac{C^2}{2} + g \cdot z \right)_{ex} \tag{20}$$

where  $E$  is the total energy of the system,  $\dot{Q}$  is the heat transfer rate,  $\dot{W}$  is the power,  $\dot{m}_{su}$  and  $\dot{m}_{ex}$  are the mass flow rates entering and leaving the system, and  $(h + \frac{C^2}{2} + g \cdot z)$  is the total enthalpy.

The mass balance across a control volume is:

$$\frac{dm}{dt} = \sum \dot{m}_{su} - \sum \dot{m}_{ex} \tag{21}$$

By neglecting the kinetic and potential energies, the total energy of the system is the internal energy of the fluid  $U$  and the left-hand side of Equation (20) can be written as:

$$\frac{dE}{dt} = \frac{dU}{dt} = m \cdot \frac{du}{dt} + u \cdot \frac{dm}{dt} \tag{22}$$

The goal of the following development is to express the derivative of the temperature. Indeed, the derivatives of the temperature and the mass allow, knowing the volume by Equation (12), computation of the temperature and the specific volume of the fluid inside the cylinder. Since the development is different if the fluid is superheated or saturated, the two cases are considered, allowing the model to simulate a potential condensation of the fluid inside the cylinder.

In the single-phase case, combining Equations (21) and (22) and considering that:

- The change of specific internal energy of an open control volume is:

$$du = c_v \cdot dT + \left[ T \left( \frac{\partial P}{\partial T} \right)_v - P \right] \cdot dv \tag{23}$$

- The specific internal energy can be expressed as:

$$u = h - P \cdot v \tag{24}$$

- Assuming uniform pressure inside the control volume, the power is:

$$\dot{W} = -P \cdot \frac{dV}{dt} \tag{25}$$

Equation (20) can be rewritten as:

$$m \cdot c_v \cdot \frac{dT}{dt} + T \cdot \left( \frac{dP}{dT} \right)_v \cdot \left[ \frac{dV}{dt} - \frac{1}{\rho} \cdot \frac{dm}{dt} \right] + h \cdot \frac{dm}{dt} = \dot{Q} + \sum \dot{m}_{su} \cdot h_{su} - \sum \dot{m}_{ex} \cdot h_{ex} \tag{26}$$

And finally, as  $h_{ex} = h$  and applying the variable change  $d\theta = \omega \cdot dt$ , the derivative of the temperature with respect to the shaft angle can be expressed as:

$$\frac{dT}{d\theta} = \frac{1}{m \cdot c_v} \cdot \left[ -T \cdot \left( \frac{\partial P}{\partial T} \right)_v \cdot \left( \frac{dV}{d\theta} - v \cdot \frac{dm}{d\theta} \right) + \frac{\dot{Q}}{\omega} + \sum \frac{\dot{m}_{su}}{\omega} \cdot (h_{su} - h) \right] \tag{27}$$

In this equation, the heat transfer is the heat brought to the fluid, thus  $\dot{Q} = -\dot{Q}_w$  [see Equation (15)], and the different mass flow rates are computed with Equation (17).

A similar type of development can be made if the fluid is saturated. Liu and Soedel, 1995 have shown that the derivative of the temperature can be expressed as:

$$\frac{dT}{d\theta} = \frac{1}{a} \cdot \left[ \frac{\dot{Q}}{\omega} - \frac{h_g - h_l}{v_g - v_l} \cdot \frac{dV}{d\theta} + v \cdot \frac{h_g - h_l}{v_g - v_l} \cdot \frac{dm}{d\theta} + \sum \frac{\dot{m}_{su}}{\omega} \cdot (h_{su} - h) \right] \tag{28}$$

Where,

$$a = m \cdot \left[ x \cdot \left( \frac{dh_g}{dT} - \frac{h_g - h_l}{v_g - v_l} \cdot \frac{dv_g}{dT} \right) + (1 - x) \left( \frac{dh_l}{dT} - \frac{h_g - h_l}{v_g - v_l} \cdot \frac{dv_l}{dT} \right) - v \cdot \frac{dP}{dT} \right] \tag{29}$$

### Fluid State Equation

As mentioned hereunder, by solving the differential Equations (27) or (28) and (21), the specific volume and the temperature of the fluid in the cylinder can be computed as a function of the crank angle. In order to compute the pressure, an equation of state is needed (Equation 30). For this purpose, the CoolProp library (Bell et al., 2014) is used (CoolProp is C++ library that implements equations of state of a wide range of fluids).

$$P = P(T, v) \tag{30}$$

### Average Values

When the shaft angle evolutions of the variables of interest are known, an average can be computed over one full revolution. Considering a variable  $y(\theta)$ , its average value over one revolution is given by:

$$x = \frac{1}{2\pi} \int_{\theta=0}^{\theta=2\pi} y(\theta) \cdot d\theta \tag{31}$$

Using this equation, the average mass flow rates entering and leaving the machine and the average thermal power exchanged with the cylinder wall can be computed.

In order to compute the average exhaust temperature, the specific average exhaust enthalpy is computed by:

$$\overline{h_{ex}} = \frac{\int_{\theta=0}^{\theta=2\pi} \dot{M}_{ex}(\theta) \cdot h_{ex}(\theta) \cdot d\theta}{\int_{\theta=0}^{\theta=2\pi} \dot{M}_{ex}(\theta) \cdot d\theta} \tag{32}$$

The average exhaust temperature can be calculated considering the average exhaust enthalpy and the exhaust pressure.

Indicated power delivered by the fluid is computed by integrating the area of the indicator diagram.

### Average Energy Balance

In steady-state regime, the following energy balance can be written for the cylinder wall:

$$\dot{Q}_w + \dot{W}_{loss} = \dot{Q}_{amb} + \dot{Q}_{cooling} \tag{33}$$

where  $\dot{W}_{loss}$  is the mechanical friction loss dissipated as heat,  $\dot{Q}_{cooling}$  is the heat removed by a possible cooling system (e.g. water cooled engine) and  $\dot{Q}_{amb}$  is the ambient heat loss:

$$\dot{Q}_{amb} = AU_{amb} \cdot (T_w - T_{amb}) \tag{34}$$

### Numerical Solution Method and Model Closure

The model described above has been implemented in Matlab and the numerical solution is reached as follows. First the inputs are defined, the geometrical variables are computed, the wall temperature is guessed and an assumption on initial state of the fluid is made. Then the governing differential equations are solved using the Euler forward method. Once the evolution of the fluid state during one revolution is known, the guessed initial values are compared to final values. If convergence is not reached (Equation 35), the initial values are set to the final values until the convergence is achieved.

$$\rho(0) - \rho(2\pi) < \varepsilon \tag{35}$$

Then the wall energy balance (Equation 33) is checked and if the convergence is not reached,  $T_w$  is adjusted by the bisection method until it converges. Finally, average values are computed.

### COMPREHENSIVE MODEL VALIDATION AND ANALYSIS

In this section, the comprehensive model proposed hereinabove is used to represent the tested expander. First, the geometrical parameters must be described. Then calibration parameters are adjusted to obtain the best fit between measurements and model outputs. Finally, once the model is validated, it is used to analyze the losses in more detail.

#### Geometrical Parameters

The geometrical parameters that must be defined are the evolution of the volume and surface area of the cylinder and the cross-sectional areas of the supply and exhaust ports in terms of shaft angle.

Cross-sectional areas of supply and exhaust ports can be deduced from their geometrical dimensions and (due to the “piston controlled” opening and closing nature of the ports) from the kinematic motion of the piston. The evolutions of these two sections are given in **Figure 2** (right).

#### Calibration Process

The calibration process consists in adjusting the parameters of the model in order to minimize the root-mean-square error for prediction of the indicated power, mass flow rate and discharge temperature over the whole set of tests. Varying the

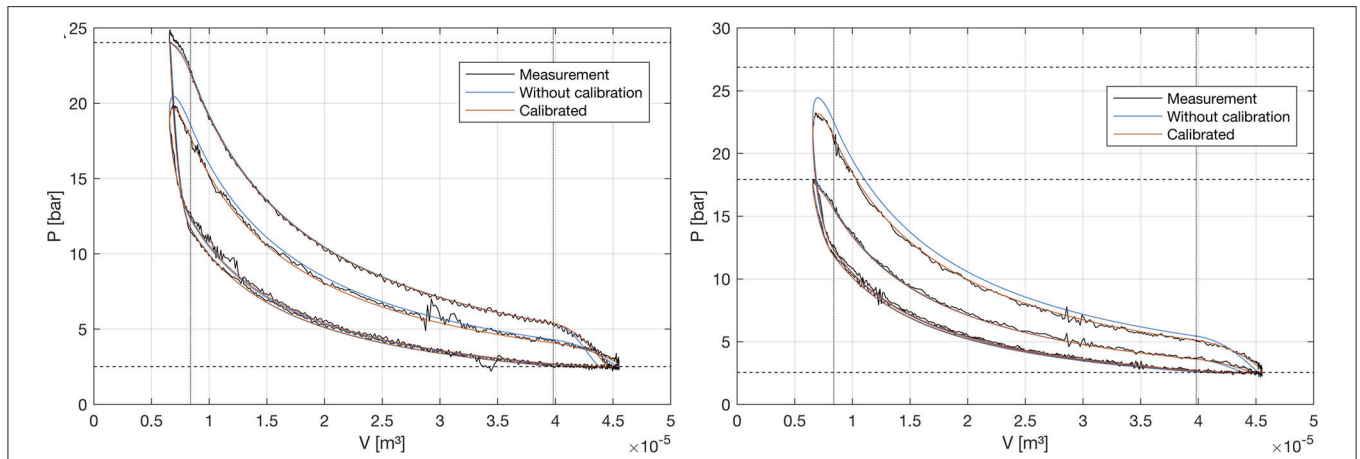


**FIGURE 9** | Comparison between measured and simulated indicator diagrams. **(left)**  $P_{ex} = 2.5$  bar,  $P_{su} = 24$  bar and  $RPM = 1,000/4,000$ ; **(right)**  $P_{ex} = 2.5$  bar,  $P_{su} = 18/27$  bar and  $RPM = 2,500$ .

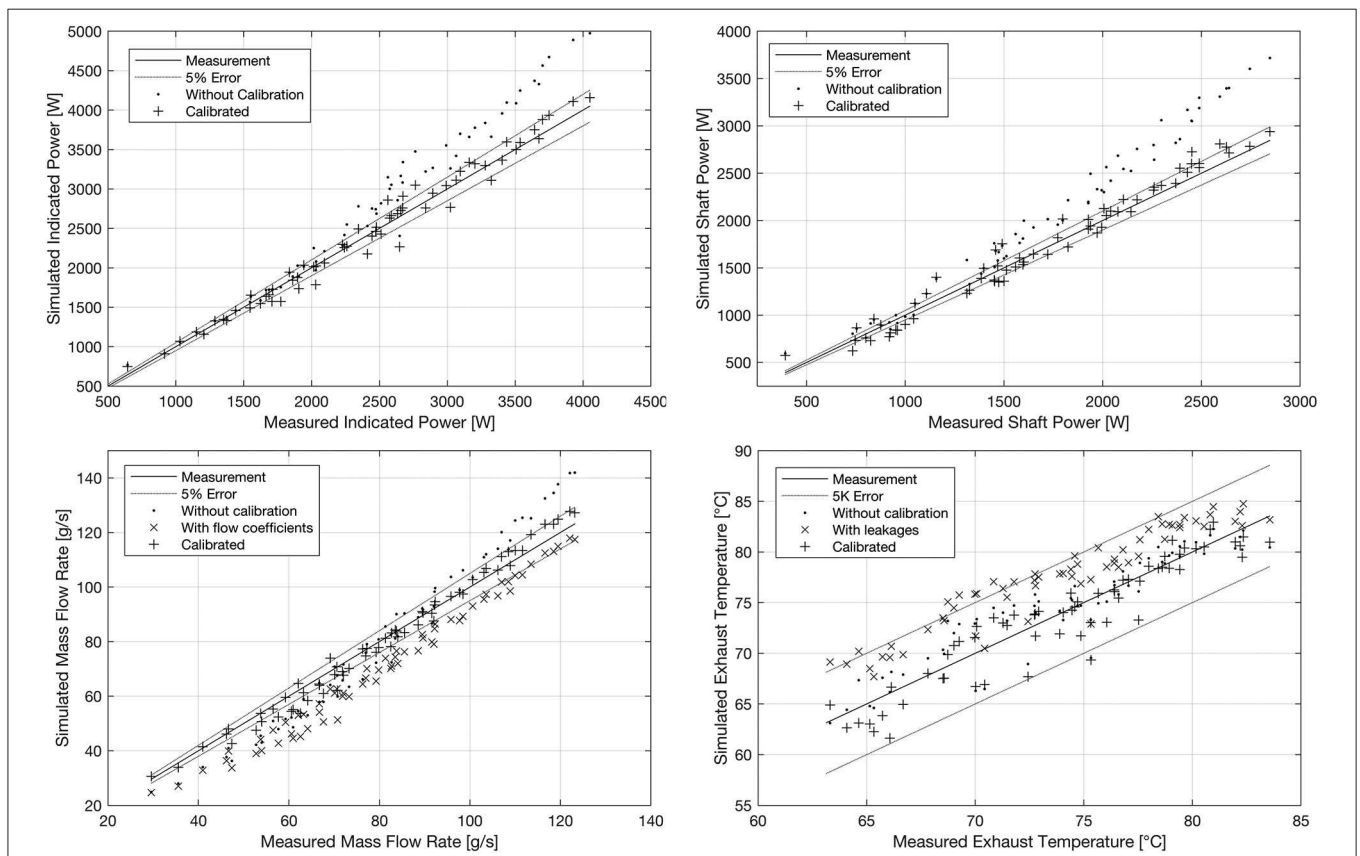


**FIGURE 10** | Comparison between measured and simulated indicated powers, shaft powers, mass flow rates, and exhaust temperatures.

flow coefficients is the only way to modify pressure drops and therefore calibrate the simulated indicator diagram.

**Figures 9, 10** (top left) show differences between some measured and simulated indicator diagrams and indicated powers, respectively. Without calibration, indicator diagrams show that the model underestimates the pressure drops and

then overestimates the indicated power. In the calibration process, flow coefficients are set to 0.82 for the supply port and 0.6 for exhaust ports in order to obtain a good fit between measured and simulated pressure curves. With these values of flow coefficients, the model is able to predict, with good accuracy, the indicated power (see **Figure 10** top left). The mechanical

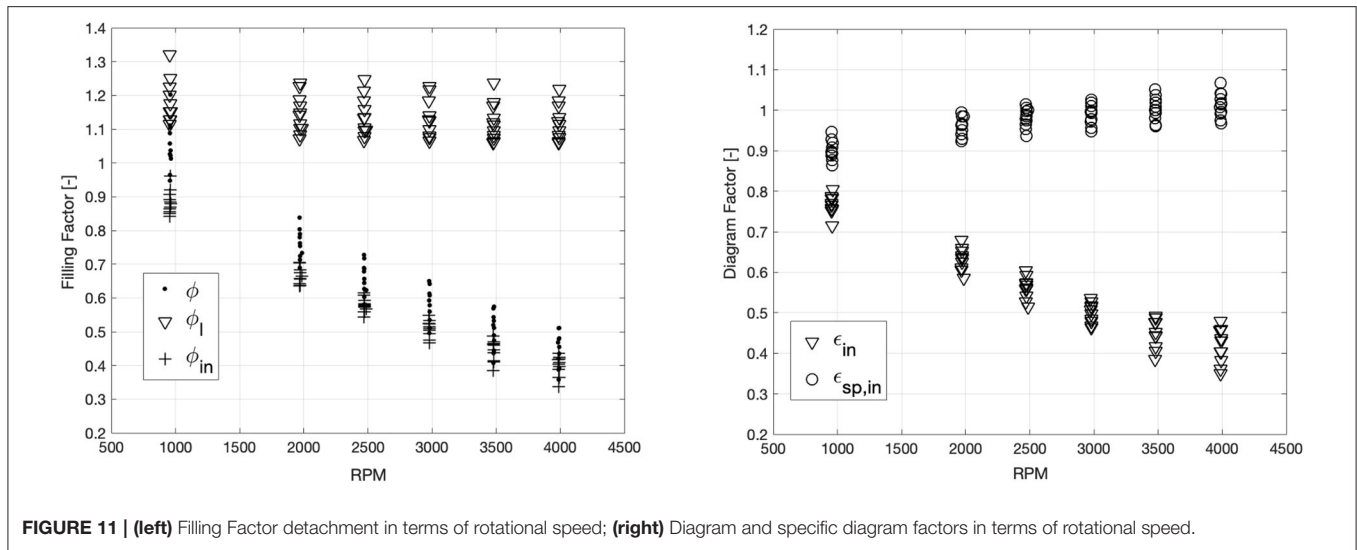


FIGURE 11 | (left) Filling Factor detachment in terms of rotational speed; (right) Diagram and specific diagram factors in terms of rotational speed.

losses are computed with Equation (10), which allows for the determination of the shaft power, as shown in Figure 10 (top right). Now that the flow coefficients are calibrated to fit the indicator diagram, Figure 10 (bottom left) shows that mass flow rate is underestimated, while exhaust temperature is still well predicted, indicating that leakages have to be added. Then the lumped leakage cross-sectional area is increased until the simulated mass flow rate fits with the measurement. Finally, the ambient heat loss coefficient is increased to obtain a better prediction of the exhaust temperature [Figure 10 (bottom right)]. The calibrated parameters are  $C_{d,su} = 0.82 [-]$ ,  $C_{d,ex} = 0.60 [-]$ ,  $A_{leak} = 0.15 [mm^2]$  and  $AU_{amb} = 3 [W K^{-1}]$ . Note that the order of magnitude of the obtained value of the ambient heat transfer coefficient can be reproduced by correlations for natural convection around a horizontal cylinder.

### Model-Based Losses Analyses

The model enables the simulation of the effect of the pressure drops/heat transfers and of the leakage separately, and subsequently the completion of the decomposition of the losses presented in section Performance Indicators. Figure 11A shows the leakage, internal and filling factors in terms of rotational speed. As expected, leakages tend to increase the filling factor (value > 1) while pressure drops tend to decrease it.

Figure 11B shows the evolution of the diagram and specific diagram factors in terms of the rotational speed. This plot shows that  $\epsilon_{sp,in}$  slightly increases with the speed, showing that pressure drops affect the mass flow rate relatively more than the internal power. The value of  $\epsilon_{sp,in}$  is close to unity (0.86–1.06).

### CONCLUSIONS

This paper presents an experimental investigation conducted on a 195 cm<sup>3</sup>, five-cylinder, swash-plate piston expander integrated into an ORC working with R245fa. 65 steady-state points, covering a large range of rotational speeds and pressure

TABLE 4 | Summary of losses analysis.

Rotational speed	$\epsilon_{s,th} [-]$	$\epsilon_{in} [-]$	$\frac{1}{\phi_{in}} [-]$	$\frac{\epsilon_{in}}{\phi_{in}} = \epsilon_{sp,in} [-]$	$\frac{1}{\phi_l} [-]$	$\epsilon_{s,in} [-]$	$\eta_m [-]$	$\epsilon_{s,sh} [-]$
1,000 RPM	0.78	0.78	1.1	0.86	0.87	0.59	0.81	0.48
2,500 PRM	0.78	0.56	1.64	0.92	0.91	0.65	0.82	0.54
4,000 RPM	0.79	0.46	2.39	1.09	0.89	0.77	0.60	0.46

ratios, were achieved. The maximal mechanical power and shaft isentropic efficiency were 2.8 kW and 53%, respectively. The measurements have been used to calibrate a model based on energy and mass conservation. The calibrated model was found to predict with a good agreement the indicated power, the shaft power, the mass flow rate and the exhaust temperature. The measurements as well as the predictions by the model have been used to analyze the performance of the expander. In order to assess the relative impact of the different sources of losses, the filling factor and shaft isentropic efficiency have been disaggregated into different factors. The impact of the rotational speed and pressure ratio has been investigated. Part of the losses analysis is summarized in Table 4, where values of factors impacting the isentropic efficiency are listed for three rotational speeds and supply and exhaust pressures of 21 bar and 2 bar, respectively (optimal operating pressures). The importance of the different sources of losses varies with the speed. For the optimal speed of 2,500 RPM, under-expansion and compression have the strongest impact, followed by mechanical losses, leakages and pressure drops, respectively.

### DATA AVAILABILITY STATEMENT

All datasets generated for this study are included in the article/Supplementary Material.

## AUTHOR CONTRIBUTIONS

J-FO conducted both the experimental and numerical research presented in this paper in the frame of his Ph.D. thesis. VL supervised the work.

## ACKNOWLEDGMENTS

The present paper is based on part of the content of the Ph.D. thesis manuscript written and defended by the J-FO (Oudkerk, 2016).

The Authors would like to thank EXOES Company for the opportunity it offered to investigate a prototype of swash plate

piston expander and Rémi Daccord for his many advice on technical issues.

## SUPPLEMENTARY MATERIAL

The Supplementary Material for this article can be found online at: <https://www.frontiersin.org/articles/10.3389/fenrg.2020.00107/full#supplementary-material>

**Supplementary Table 1** | Results of the Gaussian regression process (**top**); Minimum, maximum and average computed relative uncertainties (**bottom**).

**Supplementary Table 2** | Experimental data and expander geometrical parameters.

## REFERENCES

- Adair, R. P., Qvale, E. B., and Pearson, J. T. (1972). "Instantaneous heat transfer to the cylinder wall in reciprocating compressors," in *Proceedings of International Compressor Engineering Conference*. Purdue.
- Annand, W. J. D. (1963). Heat transfer in the cylinders of reciprocating internal combustion engines. *Proc. Instn Mech. Engrs.* 117, 973–990.
- Baek, J. S., Groll, E. A., and Lawless, P. B. (2002). "Development of a piston-cylinder expansion device for the transcritical carbon dioxide cycle" in *International Refrigeration and Air Conditioning Conference. Paper 584* (West Lafayette, IN: Purdue University). Available online at: <http://docs.lib.purdue.edu/iracc/584>
- Bao, J., and Zhao, L. (2013). A Review of working fluid and expander selections for organic rankine cycle. *Renew. Sust. Energy Rev.* 24, 325–342. doi: 10.1016/j.rser.2013.03.040
- Bell, I. H., Wronski, J., Quoilin, S., and Lemort, V. (2014). Pure and pseudo-pure fluid thermophysical property evaluation and the open-source thermophysical property library coolprop. *Ind. Eng. Chem. Res.* 53, 2498–2508. doi: 10.1021/ie4033999
- Bianchi, M., Branchini, L., Casari, N., De Pascale, A., Melino, F., Ottaviano, S., et al. (2019). Experimental analysis of a micro-ORC driven by piston expander for low-grade heat recovery. *Appl. Therm. Eng.* 148, 1278–1291. doi: 10.1016/j.applthermaleng.2018.12.019
- Blair, G. (1999). *Design and Simulation of Four-Stroke Engines*. Warrendale, PA: Society of Automotive Engineers.
- Clemente, S., Micheli, D., Reini, M., and Taccani, R. (2013). Bottoming organic rankine cycle for a small scale gas turbine: a comparison of different solutions. *Appl. Energy* 106, 355–364. doi: 10.1016/j.apenergy.2013.02.004
- Daccord, R., Darmedru, A., and Melis, J. (2014). "Oil-free axial piston expander for waste heat recovery," in *SAE Technical Paper 2014-01-0675*. doi: 10.4271/2014-01-0675
- Daccord, R., Melis, J., Kientz, T., Darmedru, A., Pieyre, R., Brisseau, N., et al. (2013). "Exhaust heat recovery with rankine piston expander," in *Société des Ingénieurs de l'Automobile*. Available online at: <http://www.sia.fr/publications/359-exhaust-heat-recovery-with-rankine-piston-expander>
- Daccord, R., and Sager, M. (2015). *A Piston Expander for Exhaust Heat Recovery on Heavy Commercial Vehicles*. AORCC: Denver, Colorado.
- Dickes, R., Dumont, O., Declaye, S., Quoilin, S., Bell, I., and Lemort, V. (2014). *Experimental Investigation of an ORC System for a Micro-Solar Power Plant*. Purdue.
- Dingel, O., Töpfer, T., and Seebode J. (2015). *Efficiency Potentials of HD Powertrains as a Function of Emissions Concept and Waste Heat Recovery*. AORCC: Denver, Colorado.
- Endo, T., Kawajiri, S., Kojima, Y., Takahashi, K., Baba, T., Ibaraki, S., et al. (2007). "Study on maximizing exergy in automotive engines," in *SAE Technical Paper 2007-01-0257*. doi: 10.4271/2007-01-0257
- Galindo, J., Dolz, V., Royo-Pascual, L., Haller, R., and Melis, J. (2015a). "Study of a volumetric expander suitable for waste heat recovery from an automotive IC engine using an ORC with ethanol," in *Proc. 3rd International Seminar on ORC Power Systems*. Brussels. Available online at: [http://www.asme-orc2015.be/online/proceedings/display\\_manuscript/85.htm](http://www.asme-orc2015.be/online/proceedings/display_manuscript/85.htm)
- Galindo, J., Ruiz, S., Dolz, V., Royo-Pascual, L., Haller, R., Nicolas, B., et al. (2015b). Experimental and thermodynamic analysis of a bottoming organic rankine cycle (ORC) of gasoline engine using swash-plate expander. *Energ. Convers. Manag.* 103, 519–532. doi: 10.1016/j.enconman.2015.06.085
- Galoppi, G. R., Secchi, L., Ferrari, G., Ferrara, S., and Karellas, D. (2017). Fiaschi radial piston expander as a throttling valve in a heat pump: focus on the 2-phase expansion. *Int. J. Refrig.* 82, 273–282. doi: 10.1016/j.ijrefrig.2017.06.025
- Heywood, J. B. (1988). *Internal Combustion Engine Fundamentals*. McGraw-Hill Series in Mechanical Engineering. New York, NY: McGraw-Hill.
- Howell, T., Gible, J., and Tun, C. (2011). "Development of an ORC system to improve hd truck fuel efficiency," in *Presented at the DEER Conference* (Detroit, MI).
- Latz, G. (2016). *Waste Heat Recovery from Combustion Engines Based on the Rankine Cycle*. (Ph.D. thesis), Gothenburg: Chalmers University of Technology.
- Latz, G., Andersson, S., and Munch, K. (2013). Selecting an expansion machine for vehicle waste-heat recovery systems based on the rankine cycle. *SAE Techn. Papers.* 1, 1–15. doi: 10.4271/2013-01-0552
- Latz, G., Erlandsson, O., Skare, T., and Contet A. (2015). "Water-based rankine-cycle waste heat recovery systems for engines: challenges and opportunities," in *Proc. 3rd International Seminar on ORC Power Systems*. Brussels: American Society of Mechanical Engineers (ASME).
- Lemort, V., Guillaume, L., Legros, A., Declaye, S., and Quoilin, S. (2013). "A comparison of piston, screw and scroll expanders for small scale rankine cycle systems," in *Proc. of the 3rd International Conference on Microgeneration and Related Technologies*. Napoli, Italy. Available online at: <http://hdl.handle.net/2268/147369>
- Liu, Z., and Soedel, W. (1995). A mathematical model for simulating liquid and vapor two-phase compression processes and investigating slugging problems in compressors. *HVAC&R Res.* 1, 99–109. doi: 10.1080/10789669.1995.10391312
- Oudkerk, J.-F. (2016). *Contribution to the characterization of piston expanders for their use in small-scale power production systems*. (Ph.D. thesis), Liège: University of Liège. Available online at: <http://hdl.handle.net/2268/202577>
- Seher, D., Lengenfelder, T., Gerhardt, J., Eisenmenger, N., Hackner, M., and Krinn, I. (2012). "Waste heat recovery for commercial vehicles with a rankine process," in *21st Aachen Colloquium Automobile and Engine Technology*. Aachen: RWTH Aachen University.
- Subcommittee, 65B: *Measurement and Control Devices* (2013). Thermocouples. Part 1, Part 1. International Electrotechnical Commission.

- Technologie Assesment and Evaluation Branch, (1974). *Exhaust Emission Test of the Carter Steam Car*.
- Woschni, G. (1967). A universally applicable equation for the instantaneous heat transfer coefficient in the internal combustion engine. *SAE Trans.* 76, 3065–3083. doi: 10.4271/670931
- Wronski, J. (2015). *Design and Modelling of Small Scale Low Temperature Power Cycles*. (Ph.D. thesis), Kongens Lyngby: DTU Mechanical Engineering.
- Wronski, J., Skovrup, M.-J., Elmegaard, B., Rislå, H.-N., and Haglind, F. (2012). “Design and modelling of a novel compact power cycle for low temperature heat sources,” in *Proceedings of ECOS 2012*, eds U. Desideri, G. Manfrida, and E. Sciubba. Available online at: <http://www.ecos2012.unipg.it/public/proceedings/html/SECS.html>
- Zhang, B., Peng, X., He, Z., Xing, Z., and Shu, P. (2007). Development of a double acting free piston expander for power recovery in transcritical CO<sub>2</sub> cycle. *Appl. Therm. Eng.* 27, 1629–1636. doi: 10.1016/j.applthermaleng.2006.05.034
- Conflict of Interest:** The authors declare that the research was conducted in the absence of any commercial or financial relationships that could be construed as a potential conflict of interest.

Copyright © 2020 Oudkerk and Lemort. This is an open-access article distributed under the terms of the Creative Commons Attribution License (CC BY). The use, distribution or reproduction in other forums is permitted, provided the original author(s) and the copyright owner(s) are credited and that the original publication in this journal is cited, in accordance with accepted academic practice. No use, distribution or reproduction is permitted which does not comply with these terms.